New route to toxic nitro and nitroso products upon irradiation of micropollutants mixtures containing imidacloprid: role of NOx and effect of natural organic matter

Davide Palma, Yara Arbid, Mohamad Sleiman, Pascal de Sainte-Claire, Claire Richard

New route to toxic nitro and nitroso products upon irradiation of micropollutants mixtures containing imidacloprid: role of NOx and effect of natural organic matter

Davide Palma, Yara Arbid, Mohamad Sleiman*, Pascal de Sainte-Claire, Claire Richard*

Université Clermont Auvergne, CNRS, SIGMA Clermont, Institut de Chimie de Clermont-Ferrand, F-63000 Clermont-Ferrand, France

* : Corresponding authors :

Mohamad.sleiman@sigma-clermont.fr and Claire.richard@uca.fr

Tel : +33 (0)4 73 40 71 42

Fax : +33 (0)4 73 40 77 00

ABSTRACT

In this study we reveal the capacity of imidacloprid (a neonicotinoid insecticide) to photoinduce nitration and nitrosation of three aromatic probes (phenol, resorcinol, tryptophan) in water. Using a gas-flow reactor and NOx analyzer, the production of gaseous NO/NO_2 was demonstrated during irradiation (300-450 nm) of imidacloprid (10^{-4} M). Quantum calculations showed that formation of NOx proceeds via homolytic cleavage of the $RN-NO_2$ bond in the triplet state. In addition to gaseous NO/NO_2, nitrite and nitrate were also detected in water, with the following mass balance: 40±8% for NO_2, 2±0.5% for NO, 52±5% for NO_3^- and 16±2% for NO_2^-. The formation of nitro/nitroso probe derivatives was evidenced by high resolution mass spectrometry and their yields were found be ranging between 0.08% and 5.1%. The contribution of NO_3^-/NO_2^- to the nitration and nitrosation processes was found minor under our experimental conditions. In contrast, the addition of natural organic matter (NOM) enhanced significantly the yields of nitro/nitroso derivatives, likely via production of

triplet excited states (^{3}NOM*) and HO$^{\cdot}$. These findings reveal the importance of investigating the photochemical reactivity of water contaminants in mixture to better understand the cocktail effects on their fate and toxicity.

Graphical abstract

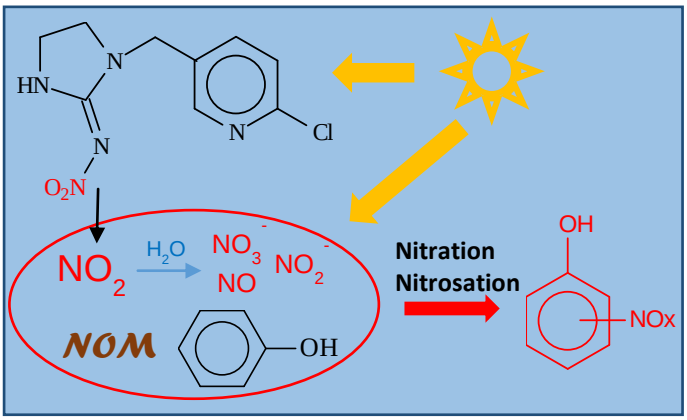

INTRODUCTION

Imidacloprid (1-[(6-chloropyridin-3-yl)methyl]-N-nitro-imidazolidin-2-imine, IMD, Scheme 1) is a widely used and effective neonicotinoid insecticide.[1] IMD, like other neonicotenoids, is used in a variety of crops and its applications have been recently extended to domestic sector and animal health.[1] Once released in the environment, it can reach the aquatic, atmospheric and terrestrial compartments and be in contact with a lot of living organisms.[2-4] IMD affects the central nervous system of insects[5] and there are increasing concerns about its deleterious effects with confirmed toxicity for pollinators, especially bees.[6] Toxicity or adverse effects in other species has been also reported[7-9].

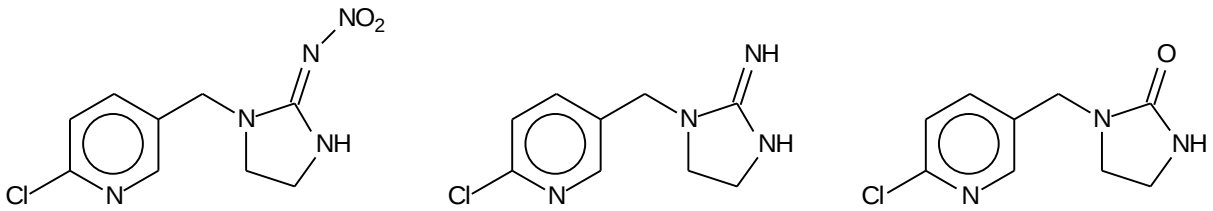

IMD desnitro-IMD urea-IMD

Scheme 1: Molecular structure of IMD and its main photoproducts

Several studies have been performed to investigate the fate of IMD under solar light, mainly in aqueous solutions[1, 10-13] on plant leaves and cuticles[14-16] and more recently on solid thin films[17]. Desnitro -IMD (1-[(6-chloropyridin-3-yl)methyl]imidazolidin-2-imine) was reported to be the main photoproduct and the urea-IMD (1-[(6-chloropyridin-3-yl)methyl]imidazolidin-2-one), a minor photoproduct (Scheme 1).[16] The formation of these by-products seems to imply the cleavage of the N-NO_2 bond; however, the fate of NO_2 is not yet clear. Recently, the formation of gaseous nitrogen oxides during the irradiation of IMD at the surface of a germanium attenuated total reflectance (ATR) crystal was investigated.[17] The

authors detected nitrous oxide (N_2O) which was proposed to be formed by recombination of detached NO_2 with the IMD fragments in the electronic ground state.

In previous studies, we showed that the fungicides chlorothalonil and thiophanate-methyl can photoinduce the degradation of other pesticides during irradiation.[18,19] These reactions can take place in surface waters where fungicides are present together with a wide range of other chemicals and on solid supports such as the surface of leaves where pesticides are often applied in combination. However, the effect that a pollutant can have on another pollutant remains largely overlooked in photochemical studies and little is known on the transformation of photostable pollutants *via* light induced reactive intermediates of other co-pollutants. The ability of IMD to release NO_2 upon irradiation makes this compound important to study in this context since nitration of chemicals have been reported in a lot of systems generating NO_2 [20-28].

The goal of this study was thus to explore the formation of reactive NOx *via* IMD photolysis and their reactivity towards surrogates of water contaminants and typical moieties of natural organic matter (phenol, resorcinol and tryptophan). In particular, we investigated the formation of nitro and nitroso-derivatives, two potentially toxic categories of compounds, from the three selected probes under polychromatic irradiation (300-450 nm) in the presence of IMD. Experiments were carried out using a flow-tube reactor equipped with NOx analyzer whereas the formation of by-products was characterized using high resolution UHPLC-ESI-MS. Theoretical calculations were also performed to elucidate the mechanisms of NOx formation. To the best of our knowledge, this is the first study reporting on the measurement of NOx during irradiation of IMD in water and on their role in nitrosation/nitration of other water pollutants. Environmental implications of this light-induced indirect degradation are discussed.

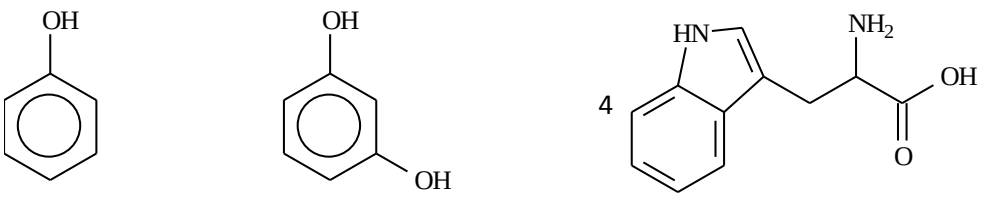

phenol resorcinol

tryptophan

Scheme 2: Selected probes

MATERIALS AND METHODS

Chemicals and materials. Imidacloprid (Pestanal®, analytical standard), resorcinol (purity 99%), phenol (purity ≥99.5%), L-tryptophan (purity ≥98%) and 2,4-dinitrophenylhydrazine (DNPH, purity 97%) were purchased from Sigma-Aldrich and used as received. Sodium nitrite (Rectapur 98%), sodium nitrate (Fluka, purity 99%), 2 and 4-nitrophenol (Fluka, purity ≥99%) and 4-nitrosophenol (Aldrich-Chemie, purity 60% due to a content of water of 40%) were also used without further purification. Suwannee River NOM (2R101N) was purchased from IHSS. Water was purified using a reverse osmosis RIOS 5 and Synergy (Millipore) device (resistivity 18 MΩ cm, DOC < 0.1 $mg.L^{-1}$). All solvents or other reactants were of the highest grade available.

Irradiations. Two different irradiation devices were used. To monitor NOx formation in the gas phase, device 1, was designed with a cylindrical Pyrex gas flow-reactor (0.65 L, length 27 cm and diameter 5.7 cm) containing 200 mL of IMD solution (10^{-4} M or 25.6 $mg.L^{-1}$) and irradiated from the top with two fluorescent tubes (Sylvania F15W/BL 368, 438 mm×26 mm, 300-450 nm, λ_{max} at 365 nm, see Figure SI-1) placed at a distance of 5 cm. The rate of incident light entering the solution was measured using a QE65000 (Ocean optics) radiometer, it was equal to 1.3×10^{16} $Photon.cm^{-2}.s^{-1}$. The gas flow-reactor was connected to a NOx chemiluminescence analyzer (Thermo Scientific i-42 NOx analyzer) as shown in Figure 1. Experiments were carried out under continuous flow of clean air, to reduce the residence time of NOx and minimize NO_2 photolysis. Gaseous inlet of the reactor was connected to flow

controllers for N_2 and O_2 (model Brooks 4800 series) allowing to select the atmosphere under which the irradiations were performed (pure N_2, pure O_2 or a 80/20 O_2/N_2 mixture) and to adjust the flow rate to 0.7 L min^{-1}. Background levels of NOx in the gas inlet were negligible (<0.4 ppbv). Before irradiation, the levels of NOx in the gas phase of the reactor were monitored continuously every 10 seconds until reaching a steady state within few minutes (Figure SI-2). Despite that NO_2 concentrations up to 40 ppbv were detected initially (first 30s), a background level of NOx (<5 ppbv) was quickly reached. This production of NO_2 might possibly be due to IMD photolysis under indoor lighting during preparation and handling of the solutions. During IMD irradiation, we have chosen to monitor NOx levels in the gas phase of the reactor at selected times and not continuously. After selected irradiation times, the light was turned off and the outlet of the reactor connected to the NOx analyzer. NOx were measured every 10 s for a period of 1-2 min at a flow rate of 0.7 L min^{-1}. The time profile of NOx concentrations shown in Figure SI-2 corresponds to the decay of NOx level in the reactor due to the dilution with clean air. The level of NOx measured was relatively constant at 1h, 2h, 4h and 6h of IMD irradiation, in accordance with a steady state regime. The levels of NOx generated were then obtained by integrating the time profiles of NOx concentrations. For calculating the yields of NOx, the ratio of NOx concentrations (ppbv) were converted into molar by taking into account the gas phase volume of the reactor (450 mL). By measuring the converted quantity (in moles) of IMD during the irradiation period, it was possible to calculate the molar yield for NO and NO_2.

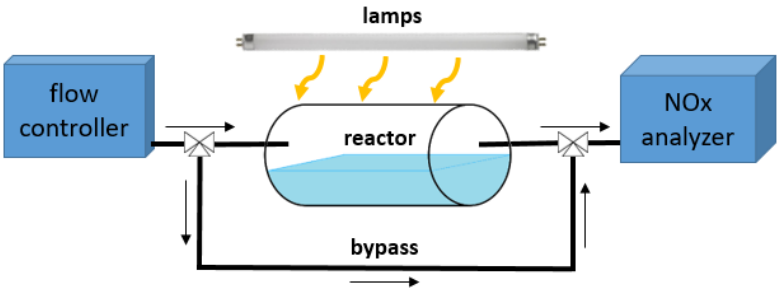

Figure 1. Schematic representation of device 1 used to monitor NOx formation upon irradiation of IMD solutions.

A second device, device 2, was used to monitor the formation of nitro and nitroso-derivatives. 15 mL of solutions were placed in a cylindrical Pyrex reactor sealed with an air-tight silicon cap and surrounded by six fluorescent tubes (Sylvania F15W/BL 368), installed inside a custom-made cylindrical irradiation device. Solutions were not buffered, but pH was controlled during the reactions. The initial pH was 6.5±0.3 and in the course of the reactions, pH laid above 5. In the case of IMD+resorcinol mixtures, aliquots were sampled after several selected irradiation times and the consumption profile of IMD and nitro- and nitroso-resorcinol were obtained. For IMD+phenol and IMD+tryptophane mixtures and experiments with nitrate/nitrite and NOM, aliquots were only sampled after 16 h of irradiation. Samples were analyzed by HPLC to monitor the loss of IMD and the probes and by UHPLC-HRMS to characterize photoproducts and estimate their levels. For the experiment at 10^{-5} M of IMD and 10^{-4} M of resorcinol, 75 ml were irradiated by portions of 25 ml, and water was evaporated up to 6 ml using a rotavapor before further analyses. Experiments were done in duplicate or triplicate. **Analytical methods.** Absorption spectra were recorded using a Varian Cary 3 spectrophotometer. IMD, phenol, resorcinol and L-tryptophan concentrations were monitored by HPLC (Waters Alliance 2695) equipped with a photodiode array detector (Waters 2996) and a EC150/4.6 Nucleodur 100-5 C_8 endcapped column. The HPLC conditions are presented in Table SI-1. was quantified using the same instrument after derivatization with DNPH.[29] 15

mL of derivatizing solution were prepared by mixing concentrated HCl, ultrapure water and acetonitrile in the ratio 2:5:1. 50 µL of this solution were added to 5 mL of sample solution. Derivatization reaction was completed in 5 min and HPLC analyses were run shortly after. Calibration used derivatized NO_2^- solutions in the concentration range 10^{-6}-10^{-5} M. All the HPLC analyses were done in triplicate and presented data are the mean values obtained.

NO_3^- was measured by ionic chromatography on a Dionex ICS-5000$^+$ using a column model Dionex Ion Pack AS11 2mm×250mm; the flow was 0.25 mL.min^{-1} and the mobile phase was an aqueous solution of KOH at the concentration of 0.43 mM for the first 4.5 min followed by a linear gradient up to 18 min of runtime by rising KOH concentration up to 11.70 mM. The injection volume was 750 µL and the temperature of the column oven was set at 30°C. External standards were prepared using $NaNO_3$ in the concentration range 50-200 µg.L^{-1}. Nitro and nitroso-derivatives of phenol, resorcinol and L-tryptophan were characterized and their concentrations estimated by high resolution mass spectrometry (HRMS) performed on an Orbitrap Q-Exactive (Thermo Scientific) coupled to an ultra-high performance liquid chromatography system (UHPLC) Ultimate 3000 RSLC (Thermo Scientific). Due to the lack available standards, desnitro-IMD and minor photoproducts were tentatively identified by HRMS but quantification was not possible. Analyses were carried out both in negative (ESI$^-$) and positive (ESI$^+$) electrospray modes. The column was the same column as for HPLC-UV. The binary solvent system was composed of acetonitrile and acidified water using formic acid at 40% and 60% respectively with a flow of 1.0 mL min^{-1}. Nitro and nitroso-phenols were quantified by injection of external standards of 4-nitro and 4-nitroso-phenols at concentrations varying from 5×10^{-7} to 4×10^{-6} M (Figure SI-3). Due to commercial unavailability of nitrated derivatives, the concentrations of nitro and nitroso-resorcinols were estimated using the calibration curves of 4-nitro and 4-nitroso-phenols. The concentrations of nitro-tryptophan and nitroso-tryptophan were estimated using L-tryptophan at the concentration of 10^{-6} M as a

reference. Yields were obtained by dividing the photoproducts concentrations by the loss of IMD in concentration and by multiplying these ratios by 100.

Computational Method. Potential Energy Surfaces (PES) were investigated with the Gaussian series of programs.[30] Density Functional Theory (DFT) calculations (optimizations, frequency calculations, identification of transition states and IRC calculations) were performed at the MN12SX/6-311++G(d,p)//MN12SX/6-31+G(d,p) level of calculation. Among the large set of hybrid range-separated functionals that we tested, MN12SX[31] gave the best agreement between experimental and theoretical absorption spectra. Finally, the time dependent-DFT (TD-DFT) method was used to compute singlet excited states. Triplet state was explored with conventional self-consistent field calculations. Solvent was modeled implicitly with the Polarizable Continuum Model (PCM). Electronic energies are reported throughout (Gibb's free energies are not provided here because low vibrational modes may introduce large uncertainties in this calculation).

RESULTS AND DISCUSSION

Photolysis of IMD. The degradation profile of neutral aqueous IMD (10^{-4} M) irradiated in device 1 is shown in Figure 2. HPLC-UV and UPLC-HRMS analyses indicated that the main photoproduct was desnitro-IMD (Figure SI-4). Three minor photoproducts were also found: a compound produced by addition of an oxygen atom on IMD (IMD+O), another one produced by addition of two oxygen atoms on desnitro-IMD (desnitro-IMD+2O) and the nitroso derivative of IMD (IMD-O) as traces (Table SI-2).

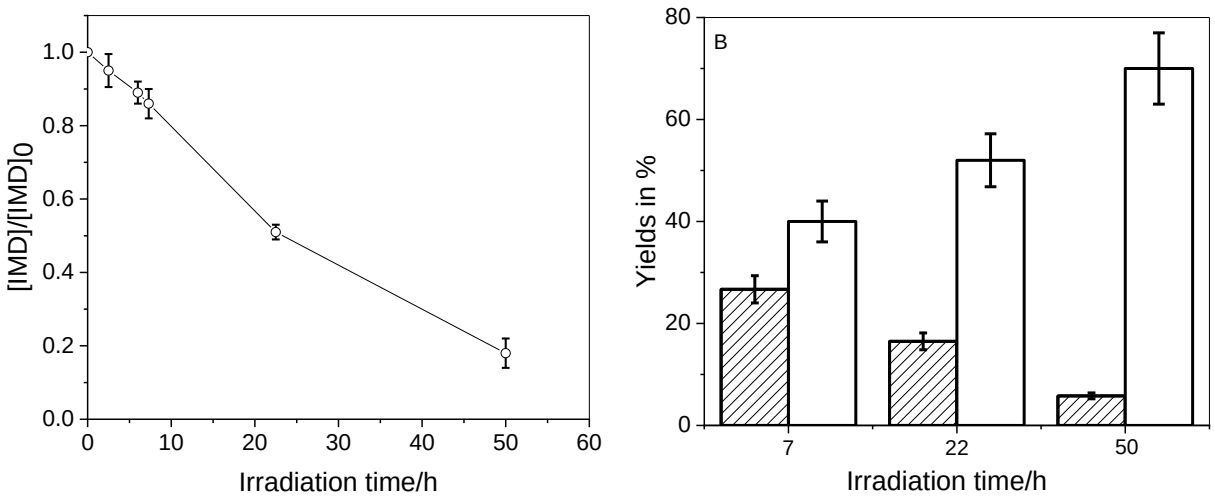

172

173 **Figure 2**. Consumption profile of aqueous IMD (10^{-4} M) irradiated in device 1 (A) and yields
174 of NO_3^- (white bars) and NO_2^- (shaded bars) (B).). Error bars are standard deviations.

175

176 NO_3^- and NO_2^- were detected in the aqueous phase (Figure SI-4). The yield of NO_3^- increased
177 constantly to reach 72±5% after 50 h of irradiation (Figure 2B, white bars). In contrast, the
178 yield of NO_2^- decreased from 27% after 7 h of irradiation to 6% after 50 h (Figure 2B, shaded
179 bars). The higher accumulation of NO_3^- compared to that of NO_2^- is consistent with the
180 spectral properties and the known photoreactivity of these ions. NO_3^- (λ_{max}= 300 nm and ε= 8
181 $M^{-1}.cm^{-1}$) absorbs much less solar light than NO_2^- (λ_{max}= 355 nm and ε= 22 $M^{-1}.cm^{-1}$) and its
182 quantum yield of photolysis is also lower (reactions 1-4) leading to a smaller photolysis rate[32]:

183 $$NO_3^- + h\nu \rightarrow NO_2 + O^{\cdot -} \quad \Phi \approx 0.01 \quad (1)$$

184 $$NO_3^- + h\nu \rightarrow NO_2^- + O(^3P) \quad \Phi \approx 0.001 \quad (2)$$

185 $$NO_2^- + h\nu + H^+ \rightarrow NO + HO^{\cdot} \quad \Phi = 0.025 \quad (3)$$

186 $$NO_2^- + h\nu \rightarrow NO_2 + e^-_{aq} \quad \Phi < 0.0019 \quad (4)$$

The detection of IMD+O and of desnitro-IMD+2O appear to be consistent with the formation of hydroxyl radicals through reactions (1) and (3).

NOx formation upon irradiation of IMD. We also measured the NOx formation in the gaseous phase above the solutions. NO and NO_2 were successfully detected upon irradiation of IMD (10^{-4} M) in device 1. Examples of collected data are shown in Figure SI-2. During the first two hours of reaction of irradiation, 24 μg of NO_2 and 0.88 μg of NO were produced whereas IMD loss was around 380 μg (See Table 2). After integrating nitrite and nitrate levels produced and considering the volume of gas (200 mL) and of water (450 mL), an overall mass balance of IMD conversion into inorganic N-containing products was determined: 40±8% for NO_2, 2±0.5% for NO, 52±5% for nitrate and 16±2% for nitrite.

Table 2. Formation of NOx after 2 h of irradiation of IMD (10^{-4} M) or mixtures NO_3^-/NO_2 in device 1.

Conditions	**Quantity of IMD converted**	**Quantity of NO_2 formed (molar yield)**	**Quantity of NO formed (molar yield)**
IMD (10^{-4} M)	380±20 μg	24±5 μg (40±8%)	0.88±0.20 μg (2±0.5%)
NO_3^- (1.8×10^{-6} M) + NO_2^- (1.7×10^{-6} M)		1.6±0.3 μg	3.9±0.8 μg
NO_3^- (2×10^{-5} M) + NO_2^- (5×10^{-6} M)		4.8±1.0 μg	11.6±2.3 μg

As the presence of NO_3^-/NO_2^- in the aqueous solution could potentially generate NO_x[33], we irradiated these ions independently to estimate their contribution to the pool of NO_x detected upon irradiation of IMD. We chose to perform these comparative experiments with NO_3^- = 1.8×10^{-6} M and NO_2^- =1.7×10^{-6} M corresponding to the concentrations estimated after 2 h of irradiation in device 1 (Figure SI-4). The irradiation of this mixture for 2 h yielded 15-fold less NO_2 and 4.4-fold more NO than the irradiation of IMD (10^{-4} M) (Table 2). The amount of NO_x formed above the IMD solution was 4.5-fold higher than that above the NO_3^-/NO_2^- solution showing that IMD was the main contributor. Moreover, the higher yield of NO in the latter system confirmed that the NO_x precursor in the NO_3^-/NO_2^- mixture was NO_2^- through reaction (3). At higher concentrations of NO_3^-/NO_2^- (2.0×10^{-5} M and 5×10^{-6} M, respectively) not far from those reached after 16h of IMD irradiation, NO and NO_2 levels were 3-fold higher than in the previous case, respectively, showing that, in this concentration range, the NO and NO_2 amounts accumulated proportionally to NO_2^- concentration. Again, the amount of NO_x generated from NO_2^- (2.0×10^{-5} M) was still below the one formed upon irradiation of IMD solution.

As previously shown, the bond N-NO_2 was cleaved when IMD was irradiated in the solid phase at 305 nm and 254 nm.[17] However, some questions remain unanswered: would the proposed mechanism in the solid phase and at short wavelength be still valid in solution and at longer wavelength, and thus at lower excitation energy? How is NO formed and how the oxygen atom is eliminated? In an attempt to answer these questions, we performed quantum calculations.

Theoretical Calculations. Several conformers were found for the solvated imidacloprid system. The structure of the global minimum was similar to that found from recent first-principles[17,34] and crystallographic investigations[34] (see SI section for all structures reported in this work). Moreover, the DFT method used here was able to reproduce accurately the experimental absorption spectrum (see Figure 3).

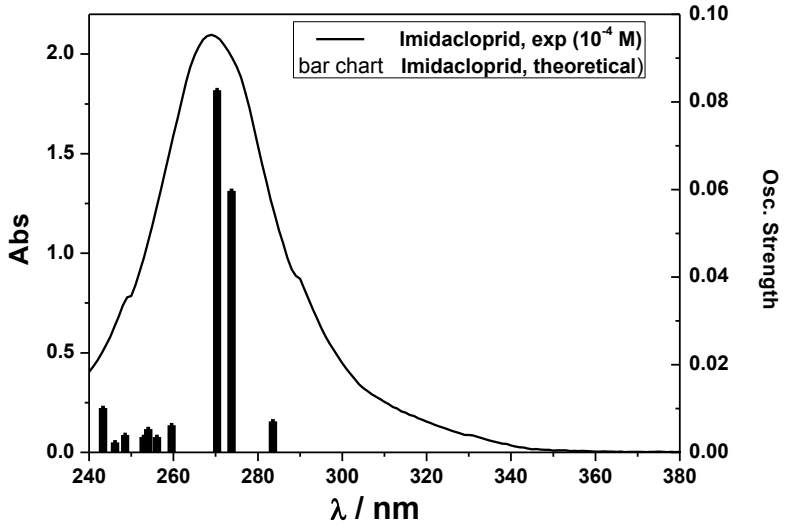

Figure 3. Experimental (Abs, left axis) and theoretical (oscillator strengths, right axis) absorption spectra of imidacloprid (theoretical spectrum for the most stable conformer (Fig. SI-5a) at the TD-MN12SX/6-311++G(d,p),PCM//MN12SX/6-31+G(d,p),PCM level. The oscillator strength is the probability of absorption. It is related to the dipole strength of the transition and is proportional to the molar absorptivity maximum for this transition. The S_1-S_0 transition is optically active (284 nm). The oscillator strength of this transition is 0.02 which is significant (an ε of about 6000 $L.mol^{-1}.cm^{-1}$ can be estimated from this value when a UV-Vis Half-Width at half-height of 0.333 eV is used to model the absorption spectrum).

Detailed investigation of the ground state (S_0), first triplet state (T_1) and first singlet excited state (S_1) was performed. Some of the key results are shown in Figure 4 and discussed below.

Minima and transition state structures are given in the SI section. The dissociation pathways of interest are depicted in this Figure: NO_2 is obtained in the left-hand side of Figure 4, and triplet atomic oxygen (a reaction that is precursor to the production of NO) is shown on the right-hand side of Figure 4. The Minimum Energy Path was followed to investigate the formation of NO_2 in S_1 by performing partial optimizations of imidacloprid for fixed RN-NO_2 bond distances. The MEP maximum is indicated by a dashed level in Figure 4.

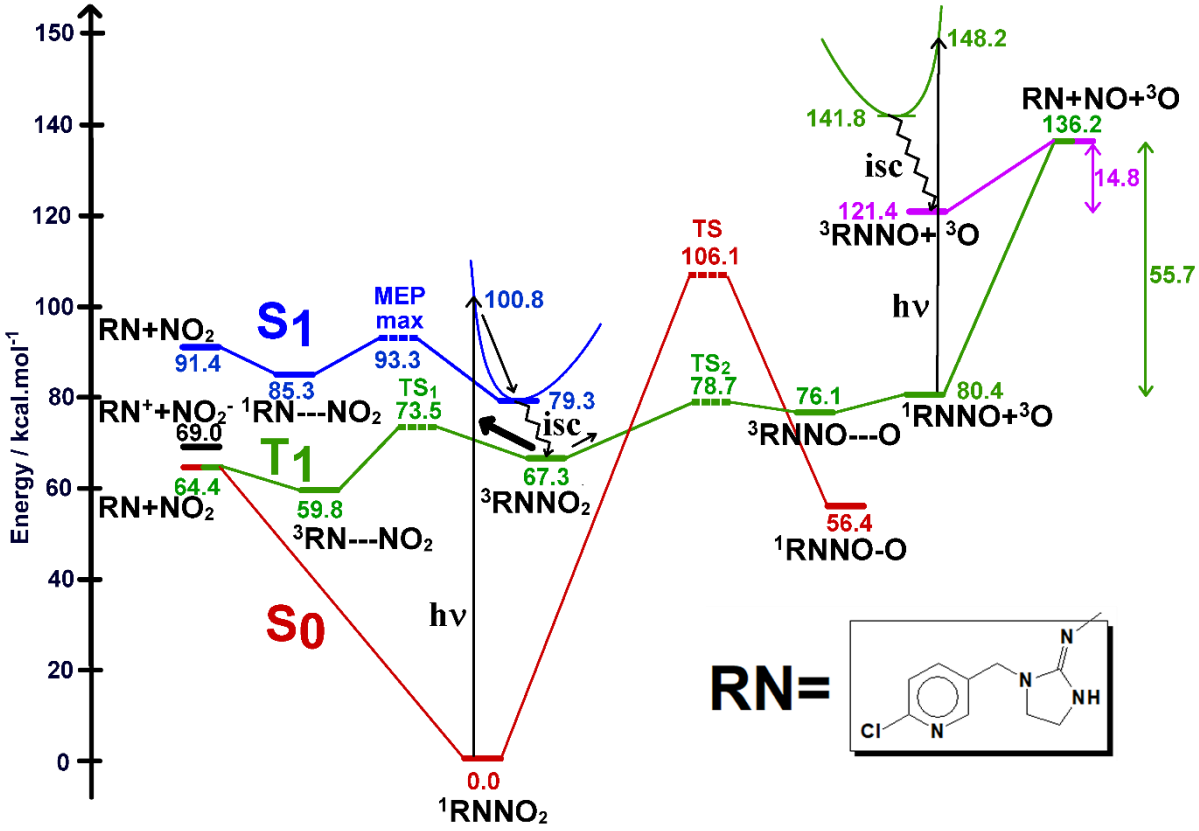

Figure 4. The electronic energies of stationary points in the ground state (S_0, red), first triplet (T_1, green) and first singlet (S_1, blue) excited states of imidacloprid (**^{1}RNNO$_2$**). Calculations were performed with the MN12SX/6-311++G(d,p),PCM//MN12SX/6-31+G(d,p),PCM method. Transition states and the MEP maximum are represented with dashed levels. Dashed bonds represent long-range separations. The energies of separated fragments **RN**+**NO$_2$** and

^{1}**RNNO**+^{3}**O** are also given in this Figure. The energy of the heterolytic dissociation products (left-hand side, black) and the triplet state of **RNNO** (right-hand side, purple) are also indicated. The separated fragments **RN** and **NO_2** in S_1 are respectively in the first doublet excited state (**RN**) and doublet ground state (**NO_2**).

S_0 and S_1 states. Our results show that departure of atomic triplet oxygen is not favored in the ground state because the predissociated intermediate ^{1}**RNNO-O** (R(O-O)=1.523 Å; 56.4 kcal.mol^{-1}) cannot be reached due to very large activation energy (106.1 kcal.mol^{-1}). Similarly, the formation of NO_2 is not expected in the ground state because the respective electronic dissociation energy in S_0 is large (64.4 kcal.mol^{-1}; **RN**+**NO_2**). A transition state could not be found between imidacloprid (^{1}**RNNO_2**) and separated radicals in S_0. This is expected for homolytic dissociations in the ground state. In S_1, the dissociation of the RN-NO_2 bond required 14.0 kcal.mol^{-1} (MEP maximum). In addition, the in-cage dissociation complex ^{1}**RN--NO_2** is less stable (85.3 kcal.mol^{-1}) than the respective reactant (79.3 kcal.mol^{-1}). Thus, dissociation in S_1 is less favored than that in the triplet state (an activation energy of 6.1 kcal.mol^{-1} was found in T_1 and the reaction is now exothermic; see Figure 4). Moreover, our results show that the heterolytic dissociation mechanism would lead to species **RN^{+}/NO_2^{-}** that are slightly less stable (see also SI) than the respective separated radicals (**RN**/**NO_2**). Thus, it seems reasonable to consider that it is the radicals that are eventually obtained in the liquid phase. However, considering the small energy difference beween heterolytic and homolytic dissociation energies, a mixture of homolytic and heterolytic dissociation products might not be completely ruled out. Implicit solvation models underestimate the solvation free energy of small ions, the cases of the proton and hydroxide being emblematic of this issue. In order to address this point, we computed $\Delta G^*_{r,calc}$ the dissociation Gibbs free energy for both heterolytic and homolytic NO_2 cleavage. In this calculation, RT×ln(24.46) was added to

279 $\Delta G^*_{r,calc}$ to account for the free energy change of 1 mol of an ideal gas from 1 atm to 1M.[35]
280 $\Delta G^0_{r,calc} = \Delta G^*_{r,calc} + RT \times \ln(24.46)$ was 58.6 and 49.2 kcal.mol^{-1} for, respectively, the
281 heterolytic and homolytic dissociation reactions, thus a difference of 9.4 kcal.mol^{-1} (recall that
282 the respective difference of electronic energies was smaller, i.e. 4.6 kcal.mol^{-1}). Considering
283 the implicit solvation model may underestimate the solvation free energy for NO_2^- by as much
284 as 10 kcal.mol^{-1}, the radical dissociated species are still more stable than the heterolytic
285 disociation fragments, in agreement with our results.
286
287 *Triplet State T_1*. Second, S_1/T_1 intersystem-crossing (*isc*) is favored because minimum
288 energy geometries in S_1 and T_1 are very similar for **RNNO$_2$** and the energy gap is small (less
289 than 0.1 kcal.mol^{-1} at the Franck-Condon geometry). In addition, in the triplet state, the barrier
290 for **NO$_2$** dissociation (6.1 kcal.mol^{-1}) is significantly smaller than that for the dissociation into
291 triplet atomic oxygen and singlet fragment (**^{1}RNNO**+**^{3}O**; 11.4 kcal.mol^{-1}), in agreement with
292 our experimental findings. Moreover, the in-cage dissociation complex **^{3}RNNO--O** is
293 thermodynamically less stable than the respective reactant **^{3}RNNO$_2$** and this reaction is
294 displaced toward the reactant. Nevertheless, this pathway was investigated below to see if this
295 reaction could play a role, even minor, in the formation of NO radicals.
296
297 *NO formation, a minor pathway*. The mechanism for production of nitric oxide from
298 **^{1}RNNO** is also shown in Figure 4. NO bond dissociation energy was 55.7 kcal.mol^{-1} for
299 **^{1}RNNO** in the ground state, whereas cleavage in the triplet state (reached through S_1 followed
300 by *isc*) required only 14.8 kcal.mol^{-1} (**RN** is obtained). A transition state could not be found in
301 T_1, and the energy of activation may be identified with the dissociation energy in that case.
302 Thus, the formation of NO as a primary product from RNNO is probably a minor pathway.

303 Thus, our quantum calculations provide strong evidence that photolysis of IMD mainly leads
304 to NO_2 formation in the overall triplet state potential energy surface while NO formation is a
305 minor pathway.
306
307 **Evidence of nitro/nitroso derivatives formation.** Nitrate and nitrite ions which generate $HO^{\cdot}$
308 radicals simultaneously with NO or NO_2 have been reported to photoinduce the nitration
309 and/or the nitrosation of phenolic derivatives.[20-24] Whether the photolysis of IMD could also
310 contribute to the formation of such toxic products was a hypothesis that we aimed to verify in
311 this study. Thus, IMD was irradiated with each of the three probes shown in Scheme 2 in a
312 small reactor (device 2) for 16 h. In these conditions, the loss of IMD irradiated alone reached
313 60% (Figure SI-7). We first compared the probes consumption (10^{-4} M) in the absence and in
314 the presence of IMD (10^{-4} M) to quantify the photoinductive effect (Table SI-4). The
315 disappearance of phenol and resorcinol were drastically faster in the presence of IMD,
316 evidencing a strong effect. Only in the case of tryptophan, the acceleration effect was small
317 due to the fast photolysis of the probe under the studied conditions.
318 Then, we monitored the formation of nitro/nitroso-derivatives by UHPLC-HRMS analyses.
319 Figure SI-8 shows the formation profile of nitroso and nitro-resorcinol upon irradiation of
320 IMD (10^{-4} M) and resorcinol (10^{-4} M). The concentration of the two photoproducts increased
321 linearly up to 7h of irradiation before reaching a plateau value after 16 h. Nitro and nitroso-
322 derivatives were also detected with phenol and tryptophan. Detected levels after 16h of
323 irradiation are given in Figure 5 (white bars) and Table SI-4. The estimated yields of nitro-
324 resorcinols reached 3.3% of converted IMD and that of nitroso-resorcinols 5.1%. The yield of
325 nitro-phenols (*ortho+para* derivatives)[21] was equal to 2.6% and that of nitroso-phenols
326 (*ortho+para* derivatives) smaller (0.5%). For tryptophan, both yields were very small,

reaching only 0.08% (nitro-derivatives) and 0.14% (nitroso-derivatives) of tryptophan converted, due to the fast direct photolysis of tryptophan.

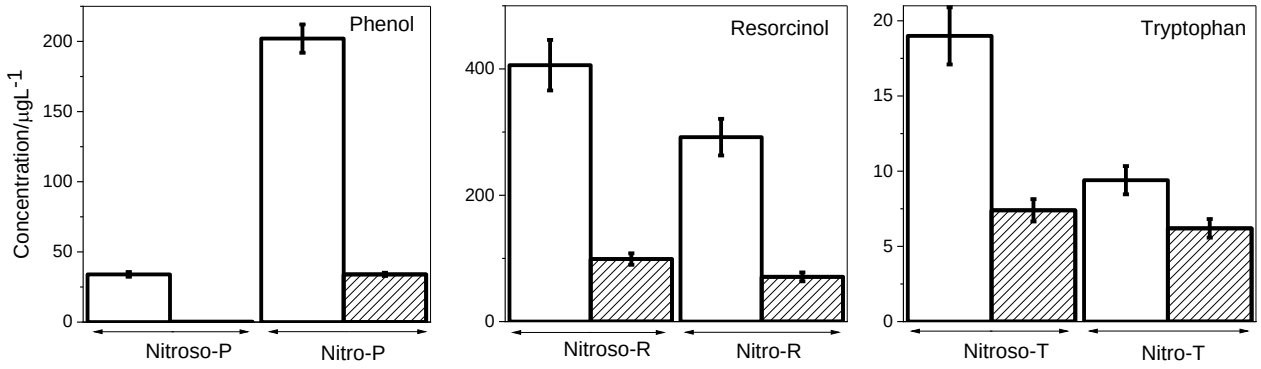

Figure 5. Concentrations of nitro and nitroso-derivatives of phenol, resorcinol and tryptophan detected after 16 h of irradiation of the probes (10^{-4} M) in device 2 in the presence of IMD (10^{-4} M) (white bars) and in presence of the mixture of NO_3^- (2×10^{-5} M) and NO_2^- (5×10^{-6} M) (shaded bars). Error bars are standard deviations.

Experiments were also performed at lower reactants concentrations to determine the impact of this parameter on the rates. A 10-fold decrease of the concentration of IMD for a concentration of resorcinol kept constant at 10^{-4} M, reduced the amount of nitro-resorcinols by 18-fold and that of nitroso-resorcinols by 9-fold while the sum of the two photoproducts was reduced by about 10-fold (Table SI-4). A 10-fold decrease of the concentration of resorcinol for a concentration of IMD kept constant at 10^{-4} M, decreased 3-fold the amount of nitro-resorcinols and 100-fold that of nitroso-resorcinols and the sum (nitro+nitroso) was reduced by about 5-fold (Table SI-4). These results indicate that the reaction rate was proportional to the concentrations of reactants. The decay rate of resorcinol followed a first order kinetic with a rate constant k that can be expressed as : $k= 5.9\times10^{-3}$ [IMD] s^{-1}.

We also studied the nitro/nitrosation capacity of the NO_3^- /NO_2^- mixture to quantify their contributions in these reactions (shaded bars in Figure 5 and Table SI-4). For these comparisons, we fixed NO_3^- /NO_2^- concentrations to those measured in the IMD solution after 16h of irradiation in device 2 (2×10^{-5} M and 5×10^{-6} M, respectively) and the mixtures NO_3^- /NO_2^- + probes were irradiated for 16 h in device 2. Nitrosation was 121-fold lower in the case of phenol, 4.1-fold in the case of resorcinol and 2.6-fold in the case of tryptophan than in the presence of IMD while nitration was 5.9-fold lower for phenol, 4.1-fold for resorcinol and 1.5-fold for tryptophan. One concludes that the contributions of NO_3^- /NO_2^- to the nitration/nitrosation processes observed in irradiated IMD solutions were minor especially for phenol and resorcinol even though we acknowledge that the conditions chosen for the comparative experiments (fixed NO_3^- /NO_2^- concentrations) cannot perfectly reproduce the dynamic and complex evolution of NO_3^- /NO_2^- during IMD irradiation.

Effect of NOM on nitration/nitrosation of probes. Another important aspect we attempted to explore is the effect of NOM on these photochemical nitration/nitrosation. Experimental conditions and results are reported in Table 3. NOM (11 $mg.L^{-1}$) increased the percentage of resorcinol loss in the presence of IMD by a factor of 2.6, after correction for the light screening effects (10%). The formation of nitroso and nitro-resorcinols in IMD solutions were increased by a factor of 1.3 and 2.0, respectively, and the formation of nitro and nitroso-resorcinols in NO_2^- solutions by factors of 35 and 2.8, respectively. The very low formation of nitro-resorcinols in the system NO_2^- +resorcinol was already shown.[20] These data highlight the significant effect of NOM on the nitro/nitroso-derivatives formation.

Table 3. Effect of NOM (11 mg.L^{-1}) on the photo-nitration/photo-nitrosation of resorcinol (10^{-4} M) after 2 h of irradiation in device 2 in the presence of IMD (10^{-4} M) or NO_2^- (5×10^{-6} M). The light screening effect of NOM (10%) is taken into account.

Conditions	% resorcinol converted	Nitroso-derivatives formed (µg.L^{-1})	Nitro-derivatives formed (µg.L^{-1})
IMD +resorcinol	7.0±0.3	83±8	44±4
IMD +resorcinol+NOM	18±1	110±10	88±9
NO_2^- +resorcinol	< 1	20±2	1±0.1
NO_2^- +resorcinol+NOM	< 1	55±5	35±3

Reaction mechanism. Many reactions are expected to take place in this complex system. The main ones are summarized below. The photolysis of IMD in water generates NO_2 in the liquid phase ($NO_{2(l)}$) together with the radical RN as shown by the quantum calculations and this latter gives rise mainly to desnitro-IMD (reaction 5). The radicals O(^{3}P) and RNNO are also produced but in much lower amounts (reaction 6). The reactivity of NO_2 in water is very high. It is reported in the literature that NO_3^- and NO_2^- are generated according reactions (7a and 7b) through the intermediary dimerisation of $NO_{2(l)}$.[36,37] NO_3^- and NO ($NO_{(l)}$) can also be produced through reaction (8).[37,38] In our experiments, $N_2O_{4(g)}$ cannot be distinguished from

$NO_{2(g)}$. Reaction (8) is probably the major NO formation pathway, but the photolysis of RNNO (reaction 11), of $NO_{2(g)}$ (reaction 12) and of NO_2^- (reaction 3) are alternative pathways for NO formation. NO is stable in water and volatilizes in the gaseous phase (reaction 9).[37] It generates $NO_{2(g)}$ by reaction with oxygen (reaction 10).

In this scheme, we did not take into account the oxidation of IMD by $HO^{\cdot}$ formed in reaction (3) because the formation of oxidation products (IMD+O) was small. NO_2^- and NO_3^- could be also oxidized by $HO^{\cdot}$.[39] However, due to the high concentration of IMD compared to those of NO_2^- and NO_3^- in the first half of the reaction, IMD and its main photoproduct desnitro-IMD are expected to be the main sinks of $HO^{\cdot}$.

$$IMD + h\nu \rightarrow NO_{2(l)} + RN \quad (5)$$

$$IMD + h\nu \rightarrow O(^3P) + RNNO \quad (6)$$

$$2NO_{2(l)} \leftrightarrow N_2O_{4(l)} \quad (7a)$$

$$N_2O_{4(l)} + H_2O \rightarrow NO_3^- + 2H^+ + NO_2^- \quad (7b)$$

$$3NO_{2(l)} + H_2O \leftrightarrow 2NO_3^- + 2H^+ + NO_{(l)} \quad (8)$$

$$NO_{(l)} \leftrightarrow NO_{(g)} \quad (9)$$

$$2NO_{(g)} + O_2 \rightarrow 2NO_{2(g)} \quad (10)$$

$$RNNO + h\nu \rightarrow NO_{(l)} + radical \quad (11)$$

$$NO_{2(g)} + h\nu \rightarrow NO_{(g)} + O(^3P) \quad (12)$$

The nitration/nitrosation of phenolic/aromatic compounds in the presence of NO_2^- or NO_3^- has been already studied. [20-25,39-41] NO_2 is recognized as having a key role in these reactions, even though the mechanisms are not fully understood. Several studies attributed the formation of phenoxyl radicals to the reaction of phenols with NO_2 [20,25,39,41] while others to their reaction

403 with $HO^{\cdot}$ [40]. Once formed phenoxyl radicals further react NO_2 to yield the ortho and para
404 derivatives of nitro-phenols. Similarly, the reaction of phenoxyl radicals with NO are
405 expected to generate nitroso-phenols. The effect of NOM on these reactions is difficult to
406 predict due to the existence of opposite reactions. Indeed, on the first hand, NOM can
407 potentially favor nitro/nitrosation reactions by generating photooxidants such as triplet excited
408 states (^{3}NOM*), singlet oxygen or $HO^{\cdot}$ that are expected to induce the formation of phenoxyl
409 radicals as shown in the literature.[39] In addition, ^{3}NOM* or $HO^{\cdot}$ could be able to oxidize NO_2^-
410 and NO_3^- into NOx[39] (see process 13 related to NO_2^-):
411
412 $$NO_2^- + {}^3NOM^*/HO^{\cdot} \rightarrow NO_2 + NOM^{\cdot -}/OH^- \qquad (13)$$
413
414 On the other hand, NOM could be also a sink for NOx due to the presence of aromatic
415 moieties in its structure and therefore could inhibit the nitration/nitrosation reaction to some
416 extent.[26,42] The overall effect of NOM will thus depend on the experimental conditions and in
417 particular on the relative concentrations of reactants. In our set-up, the presence of NOM (11
418 $mg.L^{-1}$) in IMD or NO_2^- solutions containing resorcinol (10^{-4} M) increased the amounts of
419 nitro and nitroso-resorcinols showing that in this case NOM favors the formation of the
420 phenoxyl radical and of NO_2. Since Suwannee River NOM contains 68% of fulvic acids and
421 fulvic acids contain ~3 mmol oxidizable phenol per g of carbon[43], there are about 20 µM of
422 oxidizable phenols originating from NOM in a solution containing 11 mg/l. Under these
423 conditions where the quenching molecule is in large excess over phenolic moieties in NOM, it
424 can be expected that the majority of NOM-derived photooxidants will be quenched by the
425 probe compounds to form phenoxyl radicals, which can then further react with NOx to
426 produce nitro/nitroso-phenol/resorcinol, enhancing the yields of these products as it is
427 observed.

Environmental significance. Our study showed that NOx (NO and NO_2) could be generated by irradiation of IMD and that these NOx were capable of reacting with phenolic probes to produce nitro and nitroso-derivatives. This suggests that in surface water, IMD could induce the formation of nitro and nitroso derivatives of other contaminants that could be toxicants in the aquatic environment. The importance of the phenomenon will depend on the level of IMD present in surface waters. The frequency of IMD detection in surface waters is high and concentration of IMD varies in a large range reaching 1 $\mu g.L^{-1}$ in agricultural areas.[3,4] Based on this work and on the light absorption capacities of IMD and NO_2^-, one can calculate that at 1 $\mu g.L^{-1}$, IMD could generate as much as nitroso/nitro-derivatives as NO_2^- at 0.1 $\mu g.L^{-1}$. The relative contributions of NO_2^- and IMD to nitroso/nitro-derivatives formation depend therefore on their levels in water. NO_2^- is present in surface waters at a maximal concentration of 0.1 $mg{\cdot}L^{-1}$. [44] In many cases, NO_2^- concentration will be high enough to make negligible the contribution of IMD in nitro/nitrosation reactions. However, in waters containing very low levels of NO_2^- and high levels of IMD, IMD might play a role in the nitro/nitrosation reactions.

On the other hand, we observed that NOM (11 $mg{\cdot}L^{-1}$) enhanced nitro and nitrosation reactions of phenols (10^{-4} M). The yield of nitro-resorcinol was multiplied by 2 whereas that of nitroso-resorcinol by 1.3 and when NO_2^- was used instead of IMD, the yields of nitro-resorcinol and of nitroso-resorcinol were 35-fold and 2.8-fold increased respectively. This can be explained by the enhanced formation of phenoxyl radicals in the quenching of NOM deriving photooxidants by phenols. However, this effect might be concentration-dependent. The level of NOM used in this study falls in the range of typical NOM levels found in rivers and eutrophic lakes[45], but those of probes are high. At environmentally relevant concentrations of the probe compounds (<1 µM), phenolic moieties in NOM are in excess and

it might be possible that the NOM-bound phenoxyl radicals, in higher concentration than probe -derived phenoxyl radicals might outcompete the latter for reaction with NOx. In other words, at environmentally relevant conditions, a shift towards nitration/nitrosation of NOM seems possible and the yield of nitro/nitroso-derivatives of probes could then be lower compared to the ones in the absence of NOM. The incorporation of N inorganic nitrogen (N) into NOM *via* photolysis of nitrate/nitrite and/or in advanced oxidation processes treatments was already reported and shown to generate also potentially toxic compounds.[26-28] Therefore such reactions might have also environmentally negative consequences. We could not detect any significant structural changes in NOM using HRMS analyses. Nevertheless, further experiments using N-labelled IMD or nitrite/nitrate and other hyphenated techniques may provide evidence of NOM nitration/nitrosation. Therefore, a consistent monitoring of nitro/nitroso byproducts is highly recommended to verify their potential formation.

Our study confirms the capacity of water contaminants to interact with each other under irradiation and to induce mutual degradation. Mutual effects can involve reactions between excited and ground states contaminants or the intermediary formation of reactive species like NOx in the case of IMD. Up to now, they have been poorly investigated in photochemical studies and would deserve more attention. Thus, future studies should further consider the investigation of the "cocktail effect" on the environmental fate of contaminants and more specifically the reactivity of intermediates in order to enable a more reliable monitoring of non-target pollutants and assessment of potential risks.

ASSOCIATED CONTENTS

Supporting information:

15 pages, 8 Figures and 4 Tables

Spectrum of light received by the solutions in devices 1 and 2. NOx formation in device 1 upon photolysis of IMD (10^{-4} M). Calibration curve for nitroso-phenol and for nitro-phenol. Profile of NOx, NO_3^- , NO_2^-, nitroso-resorcinol and nitro-resorcinol formations and of IMD consumption. Structure and cartesian coordinates of the minimum energy structures of IMD in S_0 (a), S_1 (b) and T_1 (c), the TS (d), intermediate RNNO-O (e) in S_0, TS_1 in T_1 (f), TS_2 in T_1 (g), ^{3}RN-NO_2 (h), ^{3}RN-NO_2 in T_1 (i), ^{1}RNNO (j) and ^{3}RNNO (k) at the B3LYP/6-311++G(d,p)//B3LYP/6-31+G(d,p) level. Minima and transition state structures with cartesian coordinates. Photo-nitration and photo-nitrosation of the probes after 16 h of irradiation in presence of IMD (10^{-5} or 10^{-4} M) or a mixture of NO_3^- (2×10^{-5} M) and NO_2^- (5×10^{-6} M). Effect of NOM (11 mg L^{-1}) on the photo-nitration/photo-nitrosation of resorcinol (10^{-4} M) after 2 h of irradiation in device 2 in the presence of IMD (10^{-4} M) or NO_2^- (5×10^{-6} M).

ACKNOWLEDGEMENTS

This paper is part of a project that has received funding from the European Union's Horizon 2020 research and innovation programme under the Marie Skłodowska-Curie grant agreement No 765860 (Aquality). The authors also thank the European Regional Development Fund of the European Union and the Région Auvergne-Rhône-Alpes for financial support under the Program "Nouveau Chercheur" (N° AV0004494) which allowed the acquisition of NOx analyzer. We thank Martin Leremboure and Guillaume Voyard (CNRS engineers), for assistance with chromatographic and mass spectrometry analyses and the anonymous reviewers who helped to improve the manuscript.

Disclaimer: The paper reflects only the author's view and that the Agency is not responsible for any use that may be made of the information it contains.

504 REFERENCES

505

506 1- Jeschke, P.; Nauen, R.; Schindler, M.; Elbert, A. Overview of the status and global strategy
507 for neonicotinoids. *J. Agric. Food Chem.* **2011**, *59 (7)*, 2897−2908. DOI:10.1021/jf101303g

508 2- Désert, M. ; Ravier, S. ; Gill, G. ; Quinapallo, A. ; Armengaud, A. ; Pochet, G. ; Savelli,
509 J.L. ; Wortham, H. ; Quivet, E. Spatial and temporal distribution of current-use pesticides in
510 ambient air of Provence-Alpes-Côte-d'Azur Region and Corsica, France. *Atmos. Environ.*
511 **2018**, *192*, 241-256. DOI:10.1016/j.atmosenv.2018.08.054

512 3- Struger, J. ; Grabuski, J. ; Cagampan, S. ; Sverko, E. ; Mcgoldrick, D. ; Marvin, C. H.
513 Factors influencing the occurrence and distribution of neonicotinoid insecticides in surface
514 waters of southern Ontario, Canada. *Chemosphere* **2017**, *169*, 516-523.
515 DOI:10.1016/j.chemosphere.2016.11.036

516 4- Hladik, M. L.; Kolpin, D. W.; Kuivila, K. M. Widespread occurrence of neonicotinoid
517 insecticides in streams in a high corn and soybean producing region, USA. *Environ. Pollut.*
518 **2014**, *193*, 189-196. DOI:10.1016/j.envpol.2014.06.033

519

520 5- Abou-Donia, M.B. ; Goldstein, L.B. ; Bullman, S. ; Tu, T. ; Khan, W.A. ; Dechkovskaia,
521 A.M. ; Abdel-Rahman, A.A. Imidacloprid induces neurobehavioral deficits and increases
522 expression of glial fibrillary acidic protein in the motor cortex and hippocampus in offspring
523 rats following in utero exposure. *J. Toxicol. Environ. Health. A.* **2008**, 71, 119-130.
524 DOI:10.1080/15287390701613140

525 6- Laycock, I. ; Lenthall, K. M. ; Barratt, A. T. ; Cresswell, J. E. Effects of imidacloprid, a
526 neonicontenoid insecticide, on reproduction in worker bumble bees (Bombus terrestris)
527 *Ecotoxicol.* **2012**, *21(7)*, 1937-1945. DOI:10.1007/s10646-012-0927-y
528
529 7- Woodcock, B.A. ; Isaac, N.J. ; Bullock, J.M. ; Roy, D.B. ; Garthwaite, D.G. ; Crowe, ;
530 Pywell R.F. Impacts of neonicotinoid use on long-term population changes in wild bees in
531 England *Nat. Commun.* **2016**, *7*, 12459. DOI:10.1038/ncomms12459

532 8- Berheim, E. H. ; Jenks, J. ; Lundgren, J. G. ; Michel, E. S. ; Grove, D. ; Jensen, W. F.
533 Effects of neonicotenoid insecticides on physiology and reproductive characteristics of
534 captive female and fawn white-tailed deer. *Sci. Rep.* **2019** *9*, 1-10. DOI:10.1038/s41598-019-
535 40994-9
536
537 9- Vesile, D. ; Suat E. Acute oxidant and inflammatory effects of imidacloprid on the
538 mammalian central nervous system. *Pestic. Biochem. Physiol.* **2010**, *97*, 13-18.
539 DOI:10.1016/j.pestbp.2009.11.008
540
541 10- Moza, P. N.; Hustert, K.; Feicht, E.; Kettrup, A. Photolysis of imidacloprid in aqueous
542 solution. *Chemosphere* **1998**, *36(3)*, 497-502. DOI:10.1016/S0045-6535(97)00359-7

543 11- Redlich, D.; Shahin, N.; Ekici, P.; Friess, A.; Parlar, H. Kinetical study of the
544 photoinduced degradation of imidacloprid in aquatic media. *Clean: Soil, Air, Water* **2007**,
545 *35(5)*, 452−458. DOI:10.1002/clen.200720014

546 12- Wamhoff, H.; Schneider, V. Photodegradation of imidacloprid. *J. Agric. Food Chem*.
547 **1999**, *47(4)*, 1730−1734. DOI:10.1021/JF980820J

548 13- Zheng, W.; Liu, W.P.; Wen, Y.Z.; Lee, S.-J. Photochemistry of insecticide imidacloprid:
549 direct and sensitized photolysis in aqueous medium. *J. Environ. Sci.* **2004**, *16(4)*, 539−542.
550 Journal Code:100967627 Netherlands

551 14- Schippers, N.; Schwack, W. Photochemistry of imidacloprid in model systems. *J. Agric.*
552 *Food Chem.* **2008**, *56 (17)*, 8023−8029. DOI:10.1021/jf801251u

553 15- Scholz, K.; Reinhard, F. Photolysis of imidacloprid (NTN33893) on the leaf surface of
554 tomato plants. *Pestic. Sci.* **1999**, *55(6)*, 652−654. DOI:10.1002/(SICI)1096-
555 9063(199906)55:6<652::AID-PS997>3.0.CO;2-I

556 16- Schippers, N.; Schwack, W. Phototransformation of imidacloprid on isolated tomato fruit
557 cuticles and on tomato fruits. *J.Photochem. Photobiol. B* **2010**, *98(1)*, 57−60.
558 doi.org/10.1016/j.jphotobiol.2009.11.004

559 17- Aregahegn, K. Z. ; Shemesh, D. ; Gerber, R. B. ; Finlayson-Pitts, B. J. Photochemistry of
560 thin solid films of the neonicotinoid imidacloprid on surfaces. *Environ. Sci. Technol.* **2017**,
561 *51(5)*, 2660−2668. doi.org/10.1021/acs.est.6b04842
562
563 18- Monadjemi, S.; Richard, C. Accelerated dissipation of the herbicide cycloxydim on wax
564 films in the presence of the fungicide chlorothalonil and under the action of solar light. *J.*
565 *Agric. Food Chem.* **2014**, *62(21)*, 4846-4851. DOI:10.1021/jf500771s

19- Kouras-Hadef, S.; Hamdache, S.; Sleiman, M.; de Sainte-Claire, P.; Richard, C. Photodegradation of the fungicide Thiophanate-methyl into a sensitizing photoproduct. *J.Photochem. Photobiol. A* **2018**, *360 (1)*, 262-269. DOI:10.1016/j.jphotochem.2018.04.046

20- Machado, F.; Boule, P. Photonitration and photonitrosation of phenolic derivatives induced in aqueous solution by excitation of nitrite and nitrate ions. *J. Photochem. Photobiol. A: Chem.* **1995**, *86(1-3)*, 73-80. DOI:10.1016/1010-6030(94)03946-R

21- Vione, D.; Maurino, V.; Pelizzetti, E.; Minero, C.. Phenol Photonitration and Photonitrosation upon Nitrite Photolysis in basic solution. *Int. J. Environ. Anal. Chem.* **2004**, *84(6-7)*, 493-504. DOI:10.1080/03067310310001640447

22- Suzuki, J.; Yagi, N.; Suzuki, S. Photochemical nitrosation of phenol in aqueous nitrite solution. *Chem. Pharm.Bull.* **1984**, *32(7)*, 2803-8. DOI:10.1248/cpb.32.2803

23- De Laurentiis, E.; Minella, M.; Berto, S.; Maurino, V.; Minero, C.; Vione, D. The fate of nitrogen upon nitrite irradiation: Formation of dissolved vs. gas-phase species. *J. Photochem. Photobiol. A: Chem.* **2015**, *307-308*, 30-34. DOI:10.1016/j.jphotochem.2015.04.005

24- Scholes, R. C.; Prasse, C.; Sedlak, D. L. The Role of Reactive Nitrogen Species in Sensitized Photolysis of Wastewater-Derived Trace Organic Contaminants. *Environ. Sci. Technol.* **2019**, *53* , 6483-6491. DOI:10.1021/acs.est.9b01386

583 25- Vione, D.; Maurino, V.; Minero, C.; Pelizzetti, E. New processes in the environmental
584 chemistry of nitrite: nitration of phenol upon nitrite photoinduced oxidation. *Environ. Sci.*
585 *Technol.* **2002**, *36*, 15, 669-676. DOI:10.1021/es010101c

586 26- Thorn, K. A.; Cox, L. G. Ultraviolet irradiation effects incorporation of nitrate and nitrite
587 nitrogen into aquatic natural organic matter. *J. Environ. Qual.* **2012**, *41(3)*, 865-881.
588 DOI:10.2134/jeq2011.0335

589 27- Yang, P.; Ji, Y.; Lu, J.; Huang, Q. Formation of nitrophenolic byproducts during heat-
590 activated peroxydisulfate oxidation in the presence of natural organic matter and nitrite.
591 *Environ. Sci. Technol.* **2019**, *53*, 4255-4264. DOI:10.1021/acs.est.8b06967

592 28- Ji, Y.; Wang, L.; Jiang, M., Lu, J.; Ferronato, C. ; Chovelon, J.-M. The role of nitrite in
593 sulfate radical-based degradation of phenolic compounds: An unexpected nitration process
594 relevant to groundwater remediation by in-situ chemical oxidation (ISCO). *Water Res.* **2017**,
595 *123*, 249-257. DOI:10.1016/j.watres.2017.06.081

596 29- Kieber, R. J.; Seaton, P. J. Determination of Subnanomolar Concentrations of Nitrite in
597 Natural Waters. *Anal. Chem.* **1995**, *67(18)*, 3261-4. DOI:10.1021/ac00114a024
598

599 30- Gaussian 09, *Revision C.01*, Frisch, M. J. ; Trucks, G. W. ; Schlegel, H. B. ; Scuseria, G.
600 E. ; Robb, M. A. ; Cheeseman, J. R. ; Scalmani, G. ; Barone, V. ; Mennucci, B. ; Petersson, G.
601 A. ; Nakatsuji, H. ; Caricato, M. ; Li, X. ; Hratchian, H. P. ; Izmaylov, A. F. ; Bloino, J. ;
602 Zheng, G. ; Sonnenberg, J. L. ; Hada, M. ; Ehara, M. ; Toyota, K. ; Fukuda, R. ; Hasegawa,
603 J. ; Ishida, M. ; Nakajima, T. ; Honda, Y. ; Kitao, O. ; Nakai, H. ; Vreven, T. ; Montgomery

Jr., J. A. ; Peralta, J. E. ; Ogliaro, F. ; Bearpark, M. ; Heyd, J. J. ; Brothers, E. ; Kudin, K. N. ; Staroverov, V. N. ; Keith, T. ; Kobayashi, R. ; Normand, J. ; Raghavachari, K. ; Rendell, A. ; Burant, J. C. ; Iyengar, S. S. ; Tomasi, J. ; Cossi, M. ; Rega, N. ; Millam, J. M. ; Klene, M. ; K nox, J. E. ; Cross, J. B. ; Bakken, V. ; Adamo, C. ; Jaramillo, J. ; Gomperts, R. ; Stratmann, R. E. ; Yazyev, O. ; Austin, A. J. ; Cammi, R. ; Pomelli, C. ; Ochterski, J. W. ; Martin, R. L. ; Morokuma, K. ; Zakrzewski, V. G. ; Voth, G. A. ; Salvador, P. ; Dannenberg, J. J. ; Dapprich, S. ; Daniels, A. D. ; Farkas, O. ; Foresman, J. B. ; Ortiz, J. V. ; Cioslowski, J. ; Fox, D. J. Gaussian, Inc., Wallingford CT, **2010**.

31- Peverati R.; Truhlar, D. G. Screened-exchange density functionals with broad accuracy for chemistry and solid state physics. *Phys. Chem. Chem. Phys.* **2012**, *14*, 16187-16191. DOI:10.1039/C2CP42576A

32- Vione, D. ; Maurino, V. ; Minero, C.; Pelizzetti , E. Reactions induced in natural waters by irradiation of nitrate and nitrite ions. *Hdb. Env. Chem.* Vol 2, Part M, Springer-Verlag Berlin (**2005**) pp 221-253.

33- Richards-Henderson, N. K.; Anderson, C.; Anastasio, C.; Finlayson-Pitts, B. J. The effect of cations on NO_2 production from the photolysis of aqueous thin water films of nitrate salts. *Phys. Chem. Chem. Phys.* **2015**, *17(48)*, 32211-32218. DOI:10.1039/C5CP05325K

34- Le Questel, J.-Y.; Graton, J.; Cerón-Carrasco, J. P.; Jacquemin, D.; Planchat, A.; Thany, S. H. New insights on the molecular features and electrophysiological properties of dinotefuran, imidacloprid and acetamiprid neonicotinoid insecticides. *Bioorg. Med. Chem.* **2011**, *19*, 7623–7634. DOI:10.1016/j.bmc.2011.10.019

627 35- Bryantsev, V. S.; Diallo, M. S.; Goddard, W. A., III Calculation of Solvation Free
628 Energies of Charged Solutes Using Mixed Cluster/Continuum Models. *J. Phys. Chem. B*
629 **2008**, *112*, 9709−9719. DOI: 10.1021/jp802665d
630

631 36- Grätzel, M. ; Henglein, A ; Lilie, J. ; Beck, G. Pulsradiolytische untersuchung einiger
632 elementarprozesse der oxydation und reduktion des nitritions. *Ber. Bunsenges. Phys. Chem.*
633 **1968**, *73* ,646-653. DOI : 10.1002/bbpc.19690730707
634

635 37- Tan, S.P.; Piri, M. Modeling the solubility of nitrogen dioxide,in water using perturbated-
636 chain statistical associating fluid theory. *Ind. Eng. Chem. Res*. **2013**, *52*, 16032-16043.
637 DOI:10.1021/ie402417p

638 38- Burdick, C. L.; Freed, E. S. The equilibrium between nitric oxide, nitrogen peroxide and
639 aqueous solution of nitric acid. *J. Am. Chem. Soc.* **1921**, *43*, 518-530.
640 DOI:10.1021/ja01436a015
641

642 39- Vione, D ; Minella, M. ; Maurino, V. ; Minero C. Indirect Photochemistry in Sunlit
643 Surface Waters: Photoinduced Production of Reactive Transient Species. *Chem. Eur. J*. **2014**,
644 *20*, 10590-10606. DOI : 10.1002/chem.201400413
645

646 40- Barzaghi, P.; Herrmann, H. A mechanistic study of the oxidation of phenol by
647 OH/NO_2/NO_3 in aqueous solution. *Phys. Chem. Chem. Phys.* **2002**, *4*, 3669-3675.
648 DOI:10.1039/b201652d

41- Alfassi, Z. B.; Huie, R. E.; Neta, P. Substituent effects on rates of one-electron oxidation of phenols by the radicals ClO_2, NO_2, SO_3^-. *J. Phys. Chem.* **1986**, *90*, 4156-4158. DOI:10.1021/j100408a063

42- Semitsoglou-Tsiapou, S.; Templeton, M.R.; Graham, N.J.D.; Mandal, S.; Hernández Leal, L.; Kruithof, J.C. Potential formation of mutagenicity by low pressure-UV/H2O2 during the treatment of nitrate-rich source waters. *Environ. Sci.: Wat. Res . Technol*. **2018**, *4 (9)*, 1252-1261. DOI:10.1039/C7EW00389G

43- Ma, H. ; Allen, H. ; Yin, Y. Characterization of isolated fractions of dissolved organic matter from natural waters and a wastewater effluent. *Wat. Res.* **2001**, 35, 985-996. DOI:10.1016/s0043-1354(00)00350-x

44- Keeney, D. ; Olson, R. A. Sources of nitrate to ground water. *Crit. Rev. Environ. Control*. **1986**, *16*, 257-304. DOI :10.1080/10643388609381748

45- Perdue, E. M. Natural organic matter in « Biogeochemistry of Inland waters », G. E. Likens (ed), Academic Press, **2009**. pp 503-516.